Diamond and Related Materials, 2 (1993) 25–35

Hydrogen dissociation in a microwave discharge for diamond deposition

C. Robert Koemtzopoulos, Demetre J. Economou* and Richard Pollard

Plasma Processing Laboratory, Department of Chemical Engineering, University of Houston, Houston, TX 77204-4792 (USA)

(Received July 30, 1992; accepted in final form October 5, 1992)

Abstract

A mathematical model was developed to predict the degree of gas dissociation in an H_2 microwave discharge sustained in a tubular reactor. Reaction rate coefficients for electron–particle reactions were determined by solving the Boltzmann equation for the electron energy distribution function (EEDF). These coefficients were parameterized and used in a plasma model to calculate the self-sustaining electric field, atomic hydrogen density and electron density in the plasma. The effects of total gas density (pressure), power, flow rate, and wall recombination probability were investigated. In the parameter range studied, gas dissociation was enhanced by lowering the total gas density and/or increasing power. Wall recombination did not affect the atom density for values of the recombination probability lower than 2×10^{-4}. Addition of 1% CH_4 to the hydrogen discharge had only a minor effect on the EEDF. Therefore, results reported here can also be used to calculate the electron–particle reaction rate coefficients in the H_2/CH_4 discharge. The model provides guidelines for controlling H_2 dissociation in plasma chemical vapor deposition reactors used for diamond growth.

1. Introduction

Diamond films have been produced by chemical vapor deposition (CVD) from C/H/O containing gases energized by hot filaments, plasmas or flames [1–5]. Despite years of intensive research, the mechanisms of diamond nucleation and growth are not well understood. It is believed that atomic hydrogen plays a key role in the process by generating the precursor radicals and/or suppressing the formation of graphite [6, 7]. There are several reports on the calculation of the atomic hydrogen concentration in hot filament CVD reactors [6, 7, and references therein]. Plasma reactors are more difficult to analyze because of the non-equilibrium nature of the discharge and the complex plasma chemistry. More specifically, the electron energy distribution function (EEDF) and electron density must be known before the atom production rate can be calculated. Therefore, it is not surprising that plasma modeling studies related to diamond deposition are scarce [8].

In plasma-activated chemical vapor deposition (PACVD) of diamond, gases are premixed and then passed through the plasma where a complex mixture of radicals, excited states and ions is generated. Deposition occurs on the substrate which is immersed in the plasma. This system is not conducive to fundamental studies of diamond deposition, since the chemical environment over the growing film is very complex and the substrate temperature is difficult to control. For this reason we are experimenting with an alternative reactor configuration which offers a well-characterized environment to study diamond film growth [9]. In this system, hydrogen (or a mixture with oxygen) is passed through the plasma. The activated gas is mixed just downstream of the plasma with the carbon-bearing gas. A temperature-controlled substrate is located beyond the mixing point. In an effort to model the reactor, we report in this paper a study of gas dissociation in a pure H_2 discharge. Studies of downstream chemistry and plasma models for H_2/O_2 mixtures will be reported later.

In current practice, the most commonly used gas mixture for PACVD of diamond is methane highly diluted in hydrogen. Since the mole fraction of methane is only a few percent, it turns out that the EEDF in the H_2/CH_4 plasma is very similar to that in pure H_2. Results for the pure H_2 discharge reported here can therefore also be used to calculate the electron–particle reaction rate coefficients in the H_2/CH_4 plasma.

2. Mathematical model

A schematic diagram of the system studied is shown in Fig. 1. A pure hydrogen discharge of length L is sustained in a cylindrical tube of radius R. The plasma is generated by applying microwave power at a frequency of 2.45 GHz. Gas flow rate and pressure can be controlled independently. The goal of this work is to

*Author to whom correspondence should be addressed.

0925-9635/93/$6.00

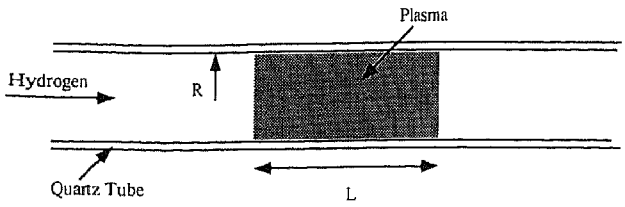

Fig. 1. Schematic diagram of a tubular reactor in which a hydrogen discharge is sustained.

calculate the atomic hydrogen density as a function of reactor geometry, wall material (atom recombination probability), and operating conditions (pressure, power, flow rate etc.).

The method of approach is as follows. First, the Boltzmann transport equation is solved for the EEDF. Electron transport properties and rate coefficients of reactions involving electrons are parameterized as a function of plasma gas composition and electric field. Then, mass and energy conservation equations are solved to determine the self-sustaining electric field, electron energy and density, and atomic hydrogen density in the discharge. Recently, this approach has also been successful in analyzing a chlorine discharge [10]. Some earlier studies of the hydrogen discharge have been reported [11]. The author, however, considered low pressure discharges (<5 Torr) assuming a Maxwellian electron energy distribution, and did not consider the effect of atomic hydrogen on the EEDF.

2.1. Electron energy distribution

The EEDF is of primary importance in the study of gas discharges because it controls the electron transport properties and the rate coefficients of electron–particle reactions. Since the degree of molecular dissociation can be quite high, the effects of both molecular and atomic hydrogen are included in the solution of the Boltzmann equation.

If E/N is weak enough so that the directed velocity of the electrons (drift velocity) is much smaller than their thermal velocity, the distribution function can be approximated by a two-term expansion in spherical harmonics. Assuming a spatially homogeneous time-independent EEDF, the Boltzmann equation reduces to [12]

$$-\frac{2}{3}\frac{\mathrm{d}}{\mathrm{d}\varepsilon}\left[\varepsilon^{3/2}\upsilon_{\mathrm{m}}(\varepsilon)\left\{\frac{e}{m}\frac{E^2}{(\upsilon_{\mathrm{m}}^2(\varepsilon)+\omega^2)}\frac{\mathrm{d}f}{\mathrm{d}\varepsilon}+\frac{3m}{M}\left(f(\varepsilon)+\frac{kT_{\mathrm{g}}}{e}\frac{\mathrm{d}f(\varepsilon)}{\mathrm{d}\varepsilon}\right)\right\}\right]=\sum_j\{\upsilon_j(\varepsilon+\varepsilon_j)f(\varepsilon+\varepsilon_j)(\varepsilon+\varepsilon_j)^{1/2}-\upsilon_j(\varepsilon)f(\varepsilon)(\varepsilon)^{1/2}\} \quad (1)$$

where ε is the electron energy, f is the EEDF, m and M are the electron and neutral mass, respectively, k is the Boltzmann constant, T_{g} is the gas temperature, ε_j is the threshold energy of process j, E is the electric field, ω is the angular frequency of the excitation field, and υ_{m} is the momentum exchange collision frequency. The collision frequency for process j is

$$\upsilon_j(\varepsilon)=N\sigma_j(\varepsilon)(2\varepsilon e/m)^{1/2} \quad (2)$$

where $\sigma_j(\varepsilon)$ is the collision cross-section and N is the neutral species density. Superelastic and electron–electron collisions are neglected in eqn. (1). The power transferred per electron is given by

$$\frac{P}{n_{\mathrm{e}}}=\frac{e^2}{m}\frac{\upsilon_{\mathrm{m}}(\varepsilon)E^2}{(\upsilon_{\mathrm{m}}^2(\varepsilon)+\omega^2)} \quad (3)$$

where P is the power and n_{e} is the electron density. In eqns. (1)–(3), υ_{m} is expressed as a function of energy ε. It can be shown using eqn. (3) that the power transfer is maximized at the resonance condition $\upsilon_{\mathrm{m}}(\varepsilon)=\omega$. Since υ_{m} is proportional to N, eqn. (1) shows that the EEDF depends on both E/N and E/ω. At the limit $\omega \gg \upsilon_{\mathrm{m}}(\varepsilon)$ the EEDF will be a function of E/ω alone (for a given gas composition). At the other extreme $\omega \ll \upsilon_{\mathrm{m}}(\varepsilon)$ the EEDF will be a function of E/N alone.

The time dependence of the EEDF is determined by the relative magnitude of the plasma excitation frequency (ω) and the electron energy and momentum relaxation frequencies [13]. If the electron energy relaxation frequency υ_{en} is much lower than ω, time modulation of the EEDF is nearly absent and a time-independent distribution is established. If, furthermore, the momentum exchange frequency υ_{m} is much higher than ω, the EEDF does not depend on the excitation frequency. For an average gas density of $5\times10^{17}\,\mathrm{cm}^{-3}$, $\omega=15.4\times10^9\,\mathrm{s}^{-1}$, $\upsilon_{\mathrm{m}}=70\times10^9\,\mathrm{s}^{-1}$, and $\upsilon_{\mathrm{en}}=0.6\times10^9\,\mathrm{s}^{-1}$. Since $\upsilon_{\mathrm{en}}<\omega<\upsilon_{\mathrm{m}}$, the EEDF is time independent and is only a function of E/N and gas composition.

In the present work, the EEDF was found using a code developed by Morgan and Penetrante [14]. The Boltzmann equation was solved for different combinations of E/N (10–70 Td; $1\,\mathrm{Td}=10^{-17}\,\mathrm{Vcm}^2$) and mole fraction of molecular hydrogen $y_{\mathrm{H_2}}$ (0.6–1.0). The distribution function was normalized so that

$$\int_0^\infty f(\varepsilon)\varepsilon^{1/2}\,\mathrm{d}\varepsilon=1 \quad (4)$$

When normalized as in eqn. (4), a Maxwellian distribution would be a straight line in a semilogarithmic plot of f *vs.* ε.

Cross-sections for vibrational excitations, electronic excitations, dissociation to excited state atoms, and ionization of H_2 as well as electronic excitations and ionization of H were obtained from Janev *et al.* [15]. The momentum transfer cross-section for H_2 was obtained from Christophorou [16], and that for H was

TABLE 1. Important reactions in a hydrogen discharge

Description	Reaction	Threshold (eV)	
Molecular ionization	$e + H_2(X^1\Sigma_g^+) \rightarrow e + H_2^+(v) + e$	15.4	[R1]
Dissociative ionization	$e + H_2(X^1\Sigma_g^+) \rightarrow e + [H_2^+(\Sigma_g \text{ and } \Sigma_u) + e] \rightarrow e + H^+ + H(1s) + e$	18.0	[R2]
Atomic ionization	$e + H(1s) \rightarrow e + H^+ + e$	13.6	[R3]
Electron–ion recombination	$e + H_3^+ \rightarrow 3H$ or $H_2(v > 5) + H^*(n = 2)$	0.0	[R4]
Dissociation to ground state H	$e + H_2(X^1\Sigma_g^+) \rightarrow e + H_2^*(a^3\Sigma_g^+, b^3\Sigma_u^+, c^3\Pi_u) \rightarrow e + H(1s) + H(1s)$	10.0	[R5]
Dissociations to excited states	$e + H_2(X^1\Sigma_g^+) \rightarrow e + H(1s) + H^*(2s)$	14.9	[R6]
	$e + H_2(X^1\Sigma_g^+) \rightarrow e + H^*(2p) + H^*(2s)$	23.0	[R7]
	$e + H_2(X^1\Sigma_g^+) \rightarrow e + H(1s) + H^*(n = 3)$	19.0	[R8]
Atomic 2p excitation	$e + H(1s) \rightarrow e + H^*(2p)$	10.2	[R9]
Atomic 2s excitation	$e + H(1s) \rightarrow e + H^*(2s)$	10.2	[R10]
Molecular excitations	$e + H_2(X^1\Sigma_g^+) \rightarrow e + H_2^*(B^1\Sigma_u^+ 2p\sigma)$	11.37	[R11]
	$e + H_2(X^1\Sigma_g^+) \rightarrow e + H_2^*(C^1\Pi_u 2p\pi)$	11.7	[R12]
	$e + H_2(X^1\Sigma_g^+) \rightarrow e + H_2^*(E, F^1\Sigma_g^+)$	12.2	[R13]
Vibrational excitations	$e + H_2(v = 0) \rightarrow e + H_2(v = 1)$	0.5	[R14]
	$e + H_2(v = 0) \rightarrow e + H_2(v = 2)$	1.0	[R15]
Volume recombinations	$H + H + H_2 \rightarrow 2H_2$		[R16]
	$H + H + H \rightarrow H + H_2$		[R17]
Wall recombination	$H + \text{Wall} \rightarrow 1/2H_2 + \text{Wall}$		[R18]

found by integrating differential cross-section data [17, 18]. Rotational excitation of H_2 was included using the "continuous approximation" of the rotational cross-section as discussed by Luft [19]. Molecular dissociation to ground state atoms occurs through three different intermediate states, $a^3\Sigma_g^+$, $b^3\Sigma_u^+$ and $c^3\Pi_u$, with threshold energies of 11.7, 8.5 and 11.7 eV respectively. These were combined into one process with a threshold of 10.0 eV [15]. Cross-sections for these collisions were obtained from the literature [20–22]. Electron–particle reactions included in the calculation are listed in Table 1. Representative cross-sections are shown in Fig. 2. Electron–electron collisions were not included since the degree of ionization of the gas was less than 10^{-6}. The rate coefficient of electron–particle reactions was determined using the EEDF and

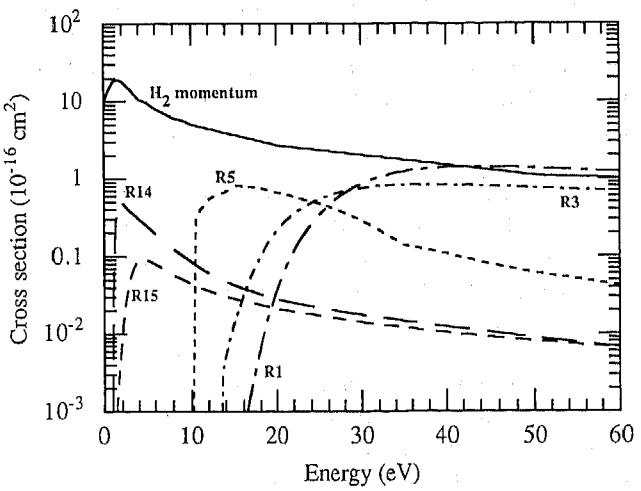

Fig. 2. Selected electron collision cross-sections for molecular and atomic hydrogen. Corresponding reactions are shown in Table 1.

$$k_j = \left(\frac{2e}{m}\right)^{1/2} \int_0^\infty \sigma_j(\varepsilon) f(\varepsilon) \varepsilon \, d\varepsilon \tag{5}$$

The mean electron energy was calculated using

$$\langle \varepsilon \rangle = \int_0^\infty f(\varepsilon) \varepsilon^{3/2} \, d\varepsilon \tag{6}$$

The rate coefficients were fitted to functions of E/N using

$$k_j = \sum_{n=0}^{5} C_n (E/N)^n \tag{7}$$

except for the molecular ionization coefficient, k_{i,H_2}, which was represented better by

$$k_{i,H_2} = C_6 \exp(-C_7/(E/N)) \tag{8}$$

The coefficients C_j $(j = 0, 7)$ were fitted to functions of y_{H_2} of the form

$$C_j = \sum_{n=0}^{3} m_n y_{H_2}^n \tag{9}$$

where m_n are constants. In the range of interest (30–50 Td and 0.8–1.0 mole fraction H_2) the fits were accurate to within 4%.

2.2. Plasma model

The plasma model consists of a system of three independent balance equations which determine the self-sustaining electric field, the electron density and the atomic hydrogen mole fraction, y_H. Since the only major components in the plasma are H_2 and H, the mole fraction of molecular hydrogen is obtained by

$y_{H_2} = 1 - y_H$. The three equations are the electron density balance, the atomic hydrogen density balance and the power balance. For the electrodeless relatively high pressure discharge examined here, secondary electron emission is not important and the plasma is sustained by bulk ionization.

The electric field and species concentrations are assumed to be uniform throughout the plasma volume. The radical density uniformity depends primarily on the wall reactivity. The radical density is expected to be uniform across the radius of the tube if diffusion is fast enough to alleviate concentration gradients. In quantitative terms, the Thiele modulus $\Phi^2 = k_w R/D_H$ must be less than unity. Here k_w is the surface recombination rate coefficient, R is the tube radius and D_H is the radical diffusivity. For the conditions of our study, $\Phi^2 < 1$ is satisfied for most situations except for unreasonably high wall reactivities.

The plasma homogeneity depends on the electric field (E) distribution. Indeed E can be non-uniform [23]. However, Ferreira *et al.* [24] have noted that an argon plasma model based on spatially averaged quantities gives nearly the same results as a more elaborate model which accounts for field inhomogeneities. In fact, the spatially average field approximation has been applied quite successfully at dc, rf and microwave frequencies [25–27]. One can account for plasma non-uniformities but the complexity of the model increases considerably. In this work we were interested in the average radical density in the discharge (to control gas dissociation) and not in the electric field distribution. Hence the use of spatially uniform average quantities is justified.

The electron density balance is considered next. Electrons are produced by ionization of molecular (reaction R1, Table 1) and atomic hydrogen (reaction R3) and they are lost by ambipolar diffusion to the walls and by electron–ion recombination (reaction R4). Hence the electron balance can be written as:

$$k_{i,H_2} N_{H_2} n_e + k_{i,H} N_H n_e = \frac{D_{ae}}{\Lambda^2} n_e + k_{e-i} n_e^2 \tag{10}$$

where n_e, N_{H_2} and N_H are the densities of electrons, molecular hydrogen and atomic hydrogen respectively, k_{i,H_2} and $k_{i,H}$ are the rate coefficients for molecular and atomic hydrogen ionization, respectively, D_{ae} is the ambipolar diffusion coefficient and Λ is the characteristic electron diffusion length. Dissociative ionization of H_2 (reaction R2), was not included because its rate was found to be two orders of magnitude lower than that of reaction R1. The assumption of electroneutrality is implicit in the last term of eqn. (10) ($n_e = n_+$, where n_+ is the positive ion density). The ambipolar diffusion coefficient is given by [28]

$$D_{ae} = D_+ \left(1 + \frac{T_e}{T_g}\right) \tag{11}$$

where D_+ is the ionic diffusion coefficient, and T_e and T_g are the electron and gas temperatures respectively. The electron temperature was based on the characteristic energy of the electrons ($\varepsilon_{char} = kT_e$), which was found through the EEDF. H_3^+ was determined to be the dominant ion in the system, and its diffusivity was obtained from McDaniel *et al.* [29] as

$$ND_+ = 2.397 \times 10^{-4} \frac{k_0 T_g}{k} \tag{12}$$

where the reduced mobility $k_0 = 11.1\ cm^2\ V^{-1}s^{-1}$. Electron impact dissociation (reaction R5) was found to be the main channel for production of H atoms. Atoms are lost by gas flow, by volume recombination (reactions R16 and R17) and by wall recombination (reaction R18). These terms of the H-atom mass balance are expressed in mathematical form as:

$$\frac{2 \times 4.48 \times 10^{17} Q_0 y_H}{(2 - y_H) V_p} = 2k_{d,H_2} N_{H_2} n_e - 2k_{v2} N_H^2 N_{H_2} - 2k_{v3} N_H^3 - \frac{2}{R} k_w N_H \tag{13}$$

where Q_0 is the feed volumetric flow rate in sccm (4.48×10^{17} is a conversion factor from sccm to molecules s^{-1}), V_p is the plasma volume and k_j (j = d, H_2, v2, v3, w) are rate coefficients for reactions R5, R16, R17, and R18 respectively. The wall recombination rate is converted to a volumetric reaction term by multiplying by the surface-to-volume ratio $2/R$, where R is the tube radius. The corresponding rate coefficient is given by

$$k_w = \frac{\gamma}{4} \sqrt{\frac{8kT_g}{\pi M_H}} \tag{14}$$

where γ is the wall recombination probability which depends critically on the condition of the surface. For the system studied axial and radial reactant concentration gradients were estimated to be small. Therefore the assumption of a well-mixed reactor is justified. The rate coefficients of reactions R16 and R17 are given by: $k_{v2} = 2.67 \times 10^{-31} T_g^{-0.6}\ cm^6\ s^{-1}$, and $k_{v3} = 1.38 \times 10^{-32}\ cm^6\ s^{-1}$, with T_g in K [6, 30, 31].

The production rate of atomic hydrogen by dissociation of vibrationally excited H_2 was also calculated by assuming a cross-section similar to that of the ground state [32] but with a threshold shifted to account for the excess energy of H_2^*. In this way, the dissociation rate coefficient was found to be slightly larger than that for dissociation of ground state molecules. However, the mole fraction of vibrationally excited molecules is expected to be around 0.01 [33], and hence the contribution of the excited state to atom production should be negligible.

The energy absorbed from the field by the electron

cloud is lost to elastic and inelastic collisions with the gas particles. At steady state, the power balance can be written as

$$\frac{P}{V_p} = \sum_j \frac{2m}{M_j} \langle \varepsilon \rangle k_{mj} n_e N_j + \sum_j \varepsilon_j k_j N_{H_2} n_e + \sum_j \varepsilon_j k_j N_H n_e + \langle \varepsilon \rangle k_{i,H_2} N_{H_2} n_e + \langle \varepsilon \rangle k_{i,H} N_H n_e \quad (15)$$

where P is the input power, $\langle \varepsilon \rangle$ is the mean electron energy, ε_j is the energy loss for the jth inelastic process, and k_j is the corresponding rate coefficient. The first term on the right-hand side (rhs) of eqn. (15) accounts for the rate at which energy is lost by the electrons through elastic collisions with atomic and molecular hydrogen. The second and third terms on the rhs represent the rate at which energy is lost via inelastic processes involving molecular and atomic hydrogen respectively. Finally, the fourth and fifth terms represent the rate at which energy is needed to bring the electrons produced by ionization to the average electron energy. The densities N_H and N_{H_2} are related by

$$N = N_H + N_{H_2} = \frac{p}{kT_g} \quad (16)$$

where N is total gas density and p is pressure.

3. Method of solution

In eqns. (10), (13) and (15) the rate coefficients of reactions involving electrons depend implicitly on E/N and y_{H_2} (or equivalently y_H). A continuation algorithm [34] was used to solve the highly non-linear system of equations. The result was the self-sustaining E/N (this is given implicitly by eqn. (10) which expresses the electron density balance for the self-sustained discharge), the H atom density, and the electron density. A parametric study was conducted by varying the total gas density, gas flow rate, power, tube radius, plasma length, and wall recombination probability.

4. Results and discussion

4.1. Electron energy distribution function

Results derived from the EEDF for 100% H_2 were compared with experimental data [35–37]. The electron characteristic energy, drift velocity, and elastic collision frequency differed by less than 20%. The dissociative excitation rate coefficient differed by less than 25% from the data of Poole [38]. These differences in electron transport properties and reaction coefficients are within experimental error, and are therefore acceptable.

Figure 3 shows typical EEDFs for 100% H_2 and for different values of E/N. The distribution functions are not Maxwellian (a Maxwellian distribution would be a straight line on this plot). The tail of the distribution function is depleted by inelastic collisions. As E/N increases, however, the tail moves to higher energy.

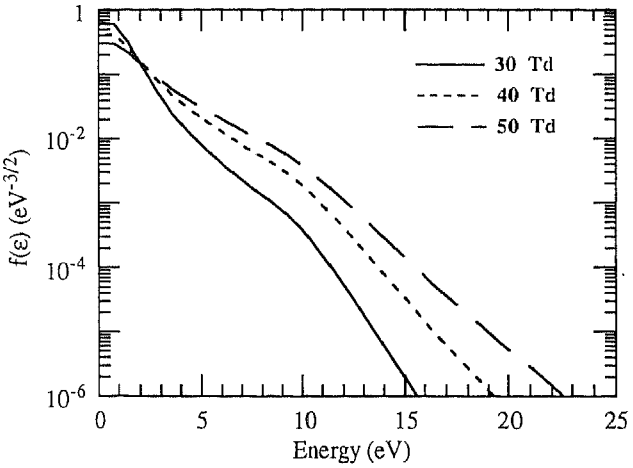

Fig. 3. Electron energy distribution function for different E/N in 100% H_2.

The distribution function can be distorted by the presence of vibrationally excited molecules [39]. However, using the results of Loureiro and Ferreira, a vibrational temperature of $T_v = 2000$ K is estimated for the present conditions. For this rather low value of T_v, the vibrational states should not have a strong influence on the EEDF. A more detailed study of the hydrogen discharge, applicable over a wider range of the parameter space, should also consider the vibrational distribution function.

The effect of mole fraction of atomic hydrogen y_H on the EEDF is shown in Fig. 4 for $E/N = 45$ Td. The tail of the distribution moves towards higher energy as y_H increases. This is because atomic hydrogen offers fewer

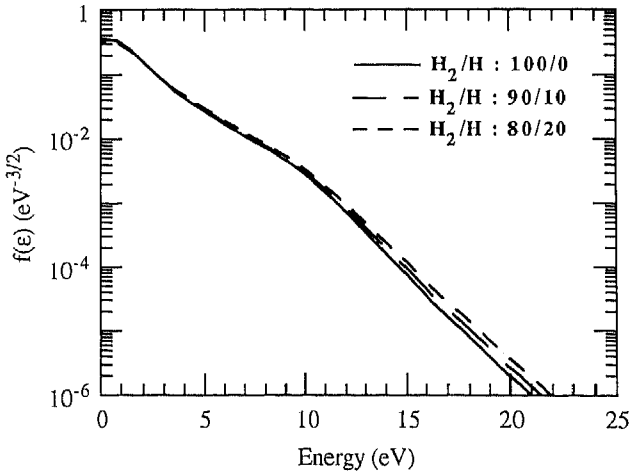

Fig. 4. Electron energy distribution function in H/H_2 mixtures with molar composition as shown and for $E/N = 45$ Td.

channels for electron energy loss. Hence the average electron energy increases with increasing y_H.

The rate coefficient for molecular hydrogen dissociation is shown in Fig. 5 as a function of E/N for different mole fractions of atomic hydrogen. The tail of the distribution shifts to higher energy by increasing either E/N (Fig. 3) or y_H (Fig. 4). Since dissociation is a tail process, the corresponding rate coefficient increases with E/N and y_H. This coefficient is of primary importance since it controls the rate of production of atomic hydrogen.

4.2. Results of plasma model

Table 2 shows the parameter values used as a base case for calculations and the range of values examined. In the figures shown below, the base values were used except when noted otherwise. Figure 6 shows the self-sustaining E/N as a function of total gas density. As density (pressure) decreases, diffusion losses of electrons to the walls of the container increase. A higher E/N is then necessary to enhance ionization and replenish the lost electrons. E/N is only slightly dependent on power. The power (electron density) dependence is a result of the non-linear (last) term in eqn. (10), and the dependence of H-atom density on power.

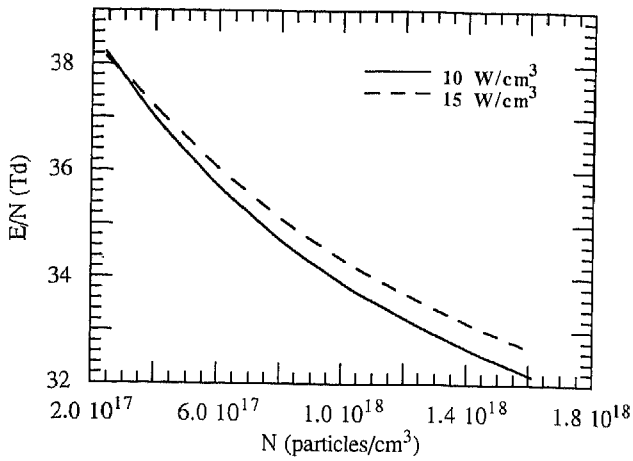

Fig. 6. Self-sustaining electric field to neutral density ratio E/N as a function of total gas density N. Other parameters were at their base value.

The H mole fraction as a function of gas density is shown in Fig. 7. As gas density increases: (a) more molecules are available for dissociation, (b) the operating E/N and therefore the rate coefficient for dissociation decreases, (c) the electron density decreases (at constant power), and (d) the atom recombination rates (reactions R16 and R17) both increase. Factors (b), (c) and (d)

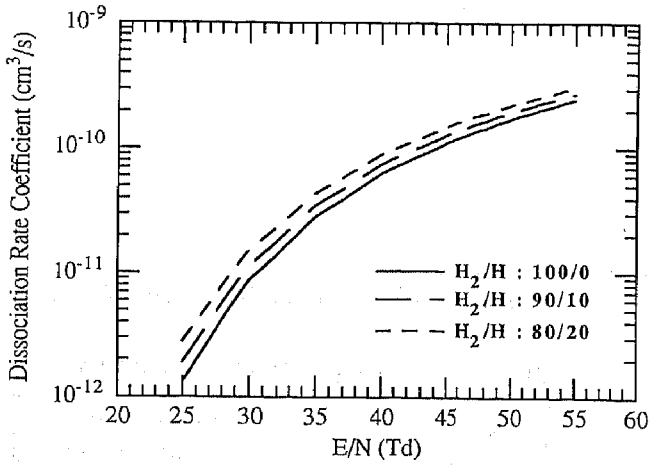

Fig. 5. Rate coefficient of H_2 dissociation as a function of E/N and for different H/H_2 mixtures.

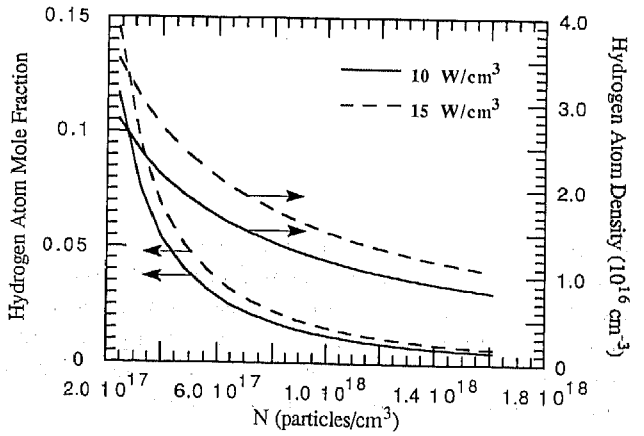

Fig. 7. Atomic hydrogen mole fraction and atomic hydrogen density as a function of total gas density N. Other parameters were at their base value.

TABLE 2. Range of parameter values studied

Name	Symbol	Range	Base value
Feed flow rate	Q_0 (sccm)	50–1000	200
Power density	P/V_p (W cm^{-3})	10.0, 15.0	10.0
Total gas density	N^a (cm^{-3})	2.5×10^{17}–1.6×10^{18}	3.18×10^{17}
Length of plasma column	L (cm)	2–10	4
Tube radius	R (cm)	1.0–2.5	1.85
Wall recombination probability	γ	0.0–2×10^{-2}	2×10^{-4}

[a]The base value for N corresponds to 20 Torr, 600 K.

more than counterbalance factor (a). The net result is a strong decline of H mole fraction with gas density. The atom density (Ny_H), however, does not decline as sharply. Figure 7 also shows that, at constant gas density, the H atom mole fraction increases with power. This is because the electron density and hence the dissociation rate increases with power.

The contribution of different terms to the electron density balance (eqn. (10)) is shown in Fig. 8. For low gas density, electron production by ionization of atomic hydrogen predominates over that of molecular hydrogen. This occurs because the atomic hydrogen mole fraction is enhanced at low N (see Fig. 7). Diffusion and electron–ion recombination are both important electron loss processes.

Atomic hydrogen loss processes are shown in Fig. 9. Volume recombination (reaction R16) is by far the dominant loss mechanism throughout the pressure range studied. On the other extreme, convection losses are negligible. Wall recombination is the second most important loss process. Of course, the relative importance of volume and wall recombination will depend on wall material and surface pretreatment. At low values of N, volume recombination (reaction R17) enters the picture since the atom density increases at lower pressures.

There is uncertainty regarding the value of the wall recombination probability γ [9]. Even if one pretreats the inside walls of the tube as suggested in the literature [40] to reduce recombination losses, the surface condition changes upon exposure to plasma. In order to assess the impact of the wall recombination probability on the atom mole fraction, a parametric study was conducted. Results are shown in Fig. 10. One observes that for values of γ less than about 2×10^{-4} the atom density is only slightly dependent on the value of γ. This suggests that other mechanisms (mainly volume recombination, Fig. 9) are more important for atom loss. As γ increases to 2×10^{-2}, however, there is strong depletion of atoms owing to wall recombination.

The most important power loss processes are shown in Fig. 11 as a function of gas density. Input power is lost mainly to vibrational excitations, since these processes have small energy threshold and large cross-sections. Power loss to molecular dissociation is the second most significant term. Power loss to elastic collisions is seen to be quite appreciable.

The effect of reactor size was also studied keeping the input power density constant. For low values of γ ($<2.0 \times 10^{-4}$), a change in tube radius did not affect y_H significantly. For high values of γ, however, increasing tube radius resulted in higher atom density because of reduced diffusion losses. For the same reason, the electron density also increased with radius. The plasma length was also varied, but its effect on the atom density was unimportant. Furthermore, it was found that flow

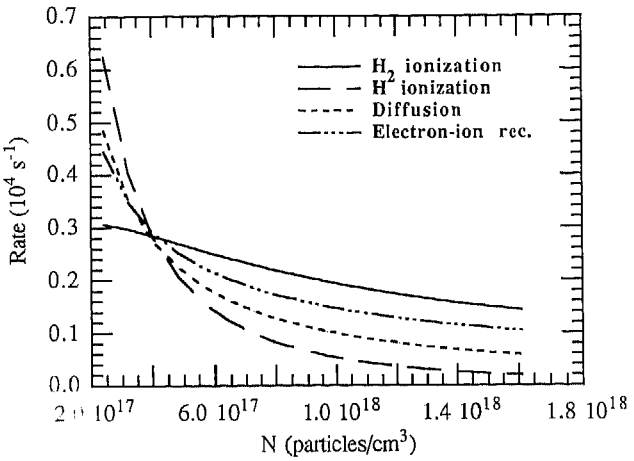

Fig. 8. Electron production and loss rates as a function of total gas density N. Other parameters were at their base value.

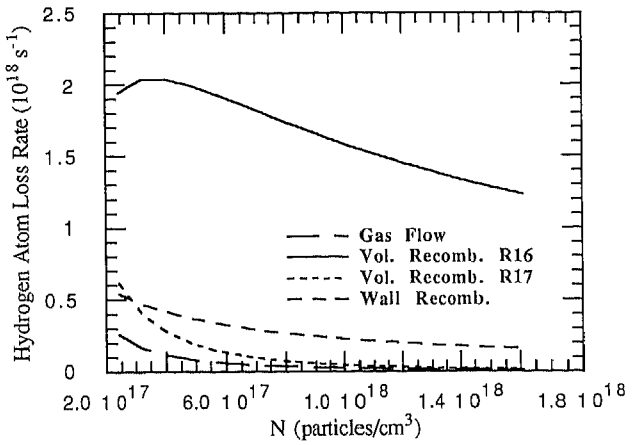

Fig. 9. Atomic hydrogen loss rates as a function of total gas density N. Other parameters were at their base value.

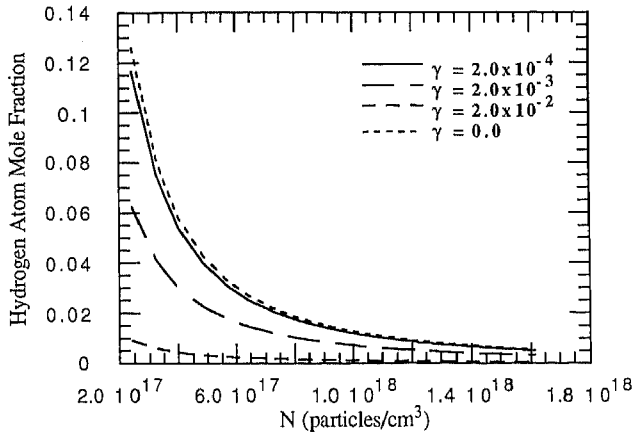

Fig. 10. Effect of the wall recombination probability γ on atomic hydrogen mole fraction as a function of total gas density N. Other parameters were at their base value.

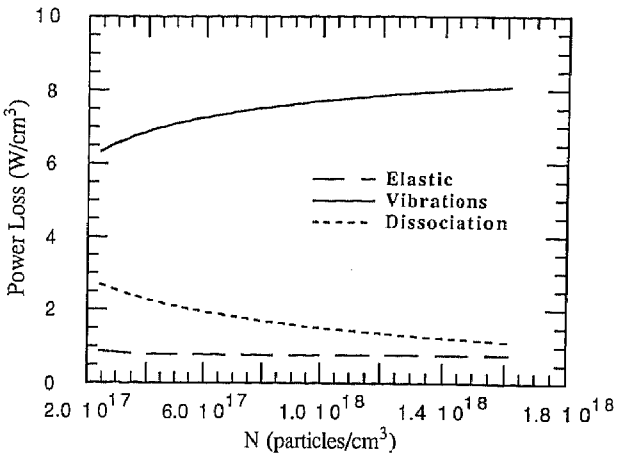

Fig. 11. Power density input to different processes as a function of total gas density N. Other parameters were at their base value.

rate variations in the range 50–500 sccm had little effect on atom density. This is because the gas residence time is long compared with molecular dissociation time constant, and also processes other than convective flow dominate the loss of atomic hydrogen (see also Fig. 9).

Last, the gas temperature was changed from 600 to 1200 K. Differences in atom mole fraction were less than 5%. This is because results are calculated in terms of gas density N and not pressure. The only places where T_g enters the calculation are eqns. (11), (12) and (14) and the rate coefficient of reaction R16. The gas temperature dependence of the ambipolar diffusivity nearly cancels out (by combining eqns. (11) and (12)), wall recombination is not a significant H atom loss process (Fig. 9), and reaction R16 does not have a strong temperature dependence. Furthermore, wall and volume recombination have opposite temperature dependencies resulting in minimal net effect of temperature. Of course in order to compare model predictions with experiment one needs to know the gas temperature, since one usually measures pressure and not gas density. The gas temperature can be calculated using an energy balance and an estimate, through the Boltzmann equation, of the plasma power which ends up as gas heating. Alternatively the gas temperature can be measured by a non-intrusive optical technique [41–43], although such measurements cannot be performed easily.

The H atom concentration has been measured using a variety of diagnostic techniques including coherent anti-Stokes Raman scattering CARS [41], 2-photon laser induced fluorescence (LIF) [42], vacuum ultraviolet (VUV) laser-absorption spectroscopy [43], and gas-phase titration using NOCl [9, 44]. Unfortunately, most plasma studies are for pressures less than 10 Torr, outside the range of the present work. Other investigators examined the high pressure regime (0.5 atm and above [45]). Surendra *et al.* [8] and Celli *et al.* [46] have studied a hydrogen plasma in a pressure range comparable to that used in our study. However, their DC plasma system differs markedly from our microwave discharge (for example, beam electrons are not expected to play a role in the microwave discharge) making comparison difficult.

4.3. CH_4 addition

The electron energy distribution function was calculated for a mixture of methane with molecular and atomic hydrogen. Cross-sections for electron impact processes of methane were taken from the literature [47–51]. Results for $H_2/H = 90/10$ and $CH_4/H_2/H = 1/90/9$ by volume are shown in Table 3 for $E/N = 40$ Td, which is a typical value of the self-sustaining field.

The electron energy and drift velocity are unaffected by adding methane, whereas the electron impact coefficients for high energy processes (excitation and ionization) are slightly different. Therefore, the EEDF calculated for pure hydrogen can also be used for evaluating electron–particle rate coefficients in a methane–hydrogen mixture. The total electron-impact dissociation rate coefficient for methane is shown in Fig. 12 (this is the dissociation rate coefficient multiplied by the electron density). Other parameters were set at their base value (Table 2) and it was assumed that the electron density does not change appreciably by the addition of 1% methane.

It is interesting to compare the plasma and thermal decomposition rates of methane. Even for a gas

TABLE 3. Comparison of electron properties and rate coefficients for two gas mixtures

	1% CH_4/90% H_2/9% H	90% H_2/10% H
Electron "temperature" (T_e, K)	19118	19094
H_2 ionization coefficient (k_{i,H_2}, $cm^3\ s^{-1}$)	1.92×10^{-14}	2.29×10^{-14}
H_2 dissociation coefficient (k_{d,H_2}, $cm^3\ s^{-1}$)	7.13×10^{-11}	7.42×10^{-11}
H ionization coefficient ($k_{i,H}$, $cm^3\ s^{-1}$)	2.8×10^{-13}	3.17×10^{-13}
CH_4 dissociation coefficient (k_{d,CH_4}, $cm^3\ s^{-1}$)	3.1×10^{-12}	3.44×10^{-12}
Characteristic energy (ε_{char}, eV)	1.73	1.73
Drift velocity (v_d, $cm\ s^{-1}$)	5.53×10^6	5.53×10^6

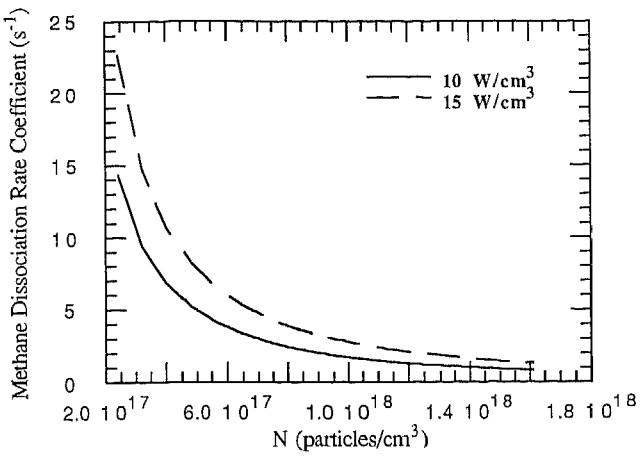

Fig. 12. Methane electron impact dissociation rate coefficient as a function of total gas density. Other parameters were at their base values.

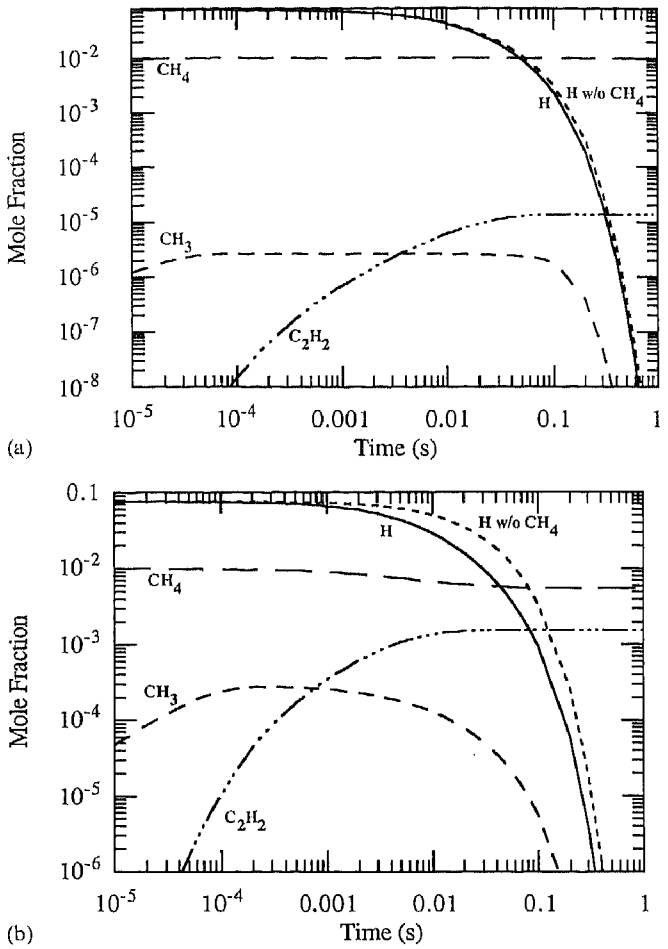

Fig. 13. Mole fraction evolution of important species downstream of the plasma. The gas stream exiting the plasma (containing H and H_2 with a mole fraction of H equal to 0.076) is mixed with 1% methane at time zero. Atomic hydrogen mole fraction without injection of methane is also shown. Conditions are 20 Torr and (a) 800 K, and (b) 1100 K.

temperature of 1200 K, the unimolecular dissociation of methane is many orders of magnitude slower than the electron impact dissociation. The hydrogen abstraction reaction ($CH_4 + H \Leftrightarrow CH_3 + H_2$), however, is 2–3 times faster than electron impact dissociation at $T_g = 600$ K, $p = 20$ Torr, and $y_H = 0.08$. This implies that it is not necessary to introduce methane into the plasma to have a substantial rate of production of methyl radicals. A high enough concentration of atomic hydrogen can initiate the methyl radical chemistry outside the plasma at relatively low temperatures. Of course, the plasma itself is necessary to produce atomic hydrogen at these low temperatures.

Figure 13 shows the concentration evolution of some important gas-phase species downstream of the plasma. The gas stream exiting the plasma contains H and H_2 with an atom mole fraction of 0.076. Added to this stream right at the plasma exit is 1% of CH_4 (this location corresponds to time zero in the figures). Other conditions were $p = 20$ Torr, and $T_g = 800$ K (Fig. 13(a)) or $T_g = 1100$ K (Fig. 13(b)). The linear velocity of the gas was 47.5 cm s^{-1} (at 1100 K). The sticking coefficient of CH_3 was assumed to be 0.03, and the wall recombination probability of H atoms was 2×10^{-4}. Other reaction rate data were found in the literature [7, 52, 53]. The atomic hydrogen concentration evolution downstream of the plasma without addition of CH_4 is also shown. The H concentration falls rapidly after about 0.1 s (corresponding to about 5 cm) mainly as a result of volume recombination reactions. Substantial concentration of methyl radicals is obtained even at low temperature and this can be enhanced by increasing temperature. In order to achieve methyl radical densities comparable to those of Fig. 13(b) in a filament CVD system, one would require temperatures in excess of 2500 K [52]. Further examination of Fig. 13 reveals that the CH_3 density also decays rapidly following the H atom decay. Assuming that CH_3 plays a major role in quality diamond growth [9, 54], the substrate must be placed within a few centimeters of the plasma to achieve good results. More detailed studies of downstream chemistry will be reported elsewhere.

5. Conclusions

A mathematical model was developed to predict the degree of gas dissociation in an H_2 microwave discharge sustained in a tubular reactor. Reaction rate coefficients for electron–particle collisions were determined by solving the Boltzmann equation for the electron energy distribution function. Electron collisions with hydrogen atoms resulting from molecular dissociation were taken into account. A system of coupled equations was solved

for the self-sustaining electric field, atomic hydrogen density and electron density in the plasma. The hydrogen atom density was calculated as a function of typical operating conditions, *i.e.*, pressure p approximately 15–100 Torr, power density about 10 W cm^{-3}, gas flow 50–500 sccm, tube radius R a few centimeters. Results can be summarized as follows:

(1) Gas dissociation as well as atom density are enhanced by lowering the total gas density and/or increasing power.

(2) Wall recombination is not an appreciable sink of hydrogen atoms for values of the recombination probability lower than 2×10^{-4}.

(3) Flow rate has a minor effect on atom density.

(4) Most of the power is consumed to vibrational excitations of molecular hydrogen. An appreciable fraction of the power goes to elastic electron–particle collisions.

(5) Addition of 1% CH_4 to the hydrogen discharge does not have any appreciable effect on the electron energy distribution function. This simplifies plasma modeling of dilute mixtures of methane in hydrogen.

(6) Methyl radical chemistry can be initiated at relatively low temperatures by injecting methane downstream of a hydrogen discharge, *i.e.*, it is not necessary to pass methane through the plasma.

Overall, the model provides guidelines for controlling H_2 dissociation in plasma chemical vapor deposition reactors used in diamond growth.

Acknowledgment

We are grateful to the State of Texas for financial support through the Texas Advanced Research Program.

References

1 P. K. Bachmann, D. Leers and H. Lydtin, *Diamond Relat. Mater., 1* (1992) 1.
2 S. Matsumoto, M. Hino and T. Kobayashi, *Appl. Phys. Lett., 51* (1987) 737.
3 *J. Mater. Res., November* (1990) (special issue on diamond CVD).
4 J. T. Glass, R. Messier and N. Fujimori (eds.), Diamond, Silicon Carbide and Related Wide Bandgap Semiconductors, *Materials Research Society Proceedings*, Vol. 162, 1989.
5 A. J. Purdes, J. C. Angus, R. F. Davis, B. M. Meyerson, K. E. Spear and M. Yoder (eds.), *Proc. Second Int. Symp. on Diamond Materials, Washington, DC, May 5–10, 1991*, The Electrochemical Society, Vol. 91–8 (1991).
6 M. Frenklach and H. Wang, *Phys. Rev. B, 43* (1991) 1520.
7 S. J. Harris and A. M. Weiner, *J. Appl. Phys., 67* (1990) 6520.
8 M. Surendra, D. B. Graves and L. S. Plano, *J. Appl. Phys., 71* (1992) 5189.
9 S. J. Harris and L. R. Martin, *J. Mater. Res., 5* (1990) 2313.
10 S. Deshmukh and D. Economou, *J. Appl. Phys., 72* (1992) 4597.
11 A. T. Bell, *Ind. Eng. Chem. Fundam., 11* (1972) 209.
12 L. L. Alves and C. M. Ferreira, *J. Phys. D: Appl. Phys., 24* (1991) 581.
13 T. Makabe and N. Goto, *J. Phys. D: Appl. Phys., 21* (1988) 887.
14 W. L. Morgan and B. M. Penetrante, *Comp. Phys. Commun., 58* (1990) 127.
JILA Information Center Report No. 19 (1979).
15 R. Janev, W. Langer, K. Evans, Jr. and D. Post, *Elementary Processes in Hydrogen–Helium Plasmas*, Springer Verlag, Berlin, 1987.
16 L.G. Christophorou (ed.), *Electron–Molecule Interactions and their Applications*, Academic Press, *1* (1983) 124.
17 J. Callaway, *Phys. Reports, 45* (1978) 89.
B. H. Bransden and M. R. C. McDowell, *Phys. Rep., 46* (1978) 249.
18 J. F. Williams, in H. Kleinpoppen and M. R. C. McDowell (eds.), *Electron and Photon Interactions with Atoms*, Plenum Press, New York, 1976, p.309.
19 P. E. Luft, *JILA Information Center Report 14*, 1975.
20 H. Tawara, Y. Hikawa, Y. Itoh, T. Kato, H. Nishimura, S. Ohtani, H. Takagi, K. Takayanagi and M. Yoshino, *Atomic Data Involving Hydrogens Relevant to Edge Plasmas*, Nagoya, Japan, 1986.
21 M. Lima, T. Gibson, W. Huo and V. McKoy, *J. Phys. B: At. Mol. Phys., 18* (1985) L865.
22 Lee Mu-Tao, R. R. Lucchese and V. McKoy, *Phys. Rev. A, 26* (1982) 3240.
S. Chung and C. C. Lin, *Phys. Rev. A, 17* (1978) 1874.
23 M. L. Passow, M. L. Brake, P. Lopez, W. B. McColl and T. E. Repetti, *IEEE Trans. Plasma Sci., 19* (1991) 219.
24 C. Ferreira, L. L. Alves, M. Pinheiro and A. B. Sa, *IEEE Trans. Plasma Sci., 19* (1991) 229.
25 E. V. Karoulina and Yu. A. Lebedev, *J. Phys. D: Appl. Phys., 25* (1992) 401.
26 M. Moisan, C. Barbeau, R. Claude, C. M. Ferreira, J. Margot, J. Paraszczak, A. B. Sa, G. Sauve and M. R. Wertheimer, *J. Vac. Sci. Technol., B9* (1991) 8.
27 A. T. Bell and K. Kwong, *AIChE J., 18* (1972) 990.
28 B. E. Cherrington, *Gaseous Electronics and Gas Lasers*, Pergamon Press, Oxford, 1979.
29 E. W. McDaniel and E. A. Mason, *The Mobility and Diffusion of Ions in Gases*, Wiley, New York, 1973.
30 J. E. Bennett, D. R. Blackmore, *Proc. R. Soc. London A., 305* (1968) 553.
31 D. L. Baulch, D. D. Drysdale, D. G. Horne and A. C. Lloyd, *Evaluated Kinetic Data for High Temperature Reactions*, Butterworths, London, *1* (1972) 266.
32 R. Celiberto, M. Cacciatore, M. Capitelli and C. Gorse, *Chem. Phys., 133* (1989) 355.
33 Yi-Fei Zhu, Yu-Lin Huang, S. Arepalli and R. J. Gordon, *J. Appl. Phys., 67* (1990) 604.
34 M. Kubicek, *ACM Transactions on Mathematical Software, 2* (1976) 98.
35 R. W. Crompton and D. J. Sutton, *Proc. R. Soc. London A, 215* (1952) 467.
36 L. Frommhold, *Z. Phys., 160* (1960) 554.
37 A. G. Robertson, *Aust. J. Phys., 24* (1971) 445.
38 H. G. Poole, *Proc. R. Soc. London A, 163* (1937) 424.
39 J. Loureiro and C. M. Ferreira, *J. Phys. D: Appl. Phys., 22* (1989) 1680.
40 A. Sepehrad, R. Marshall and H. Purnell, *Int. J. Chem. Kinetics, XI* (1979) 411.
B. J. Wood and H. Wise, *J. Phys. Chem., 65* (1961) 1976.
41 K.-H. Chen, M.-C. Chuang, C. M. Penney and W. F. Banholzer, *J. Appl. Phys., 71* (1992) 1485.
42 T. Kajiwara, K. Takeda, H. J. Kim, W. Z. Park, T. Okada, M. Maeda, K. Muraoka and M. Akazaki, *Jpn. J. Appl. Phys., 29* (1990) L154.
43 G. C. Stutzin, A. T. Young, A. S. Schlachter, J. W. Stearns, K. N. Leung and W. B. Kunkel, *Rev. Sci. Instrum., 59* (1988) 1479.

44 B. Chapman, J. Filpus, T. Morin, R. Snellenberger, J. Asmussen, H. Hawley and R. Kerber, *J. Spacecraft, 19* (1982) 579.
45 S. M. Gasworth, *Thin Solid Films, 212* (1992) 186.
46 F. G. Celli, H. R. Thorsheim, J. E. Butler, L. S. Plano and J. M. Pinneo, *J. Appl. Phys., 68* (1990) 3814.
47 Y. Ohmori, K. Kitamori, M. Shimozuma and H. Tagashira, *J. Phys. D: Appl. Phys., 19* (1986) 437.
48 D. K. Davies, L. E. Kline and W. E. Bies, *J. Appl. Phys., 65* (1989) 3311.
49 H. Chatham, D. Hils, R. Robertson and A. Gallagher, *J. Chem. Phys., 81* (1984) 1770.
50 T. E. Sharp and J. T. Dowell, *J. Chem. Phys., 46* (1967) 1530.
51 H. F. Winters, *J. Chem. Phys., 63* (1975) 3462.
52 M. Frenklach, *J. Appl. Phys., 65* (1989) 5142.
53 W. Chang and R. F. Hampson, *J. Phys. Chem. Ref. Data, 15* (1986) 1087.
54 M. P. D'Evelyn, C. J. Chu, R. H. Hange and J. L. Margrave, *Appl. Phys. Lett., 71* (1992) 1528.